Indian J. Phys. **80** (5), 471-486 (2006)

IJP

Confocal laser scanning microscopy and laser light scattering : applications in soft matter and technological materials

Baldev Raj and B V R Tata*

Metallurgy and Materials Group, Indira Gandhi Centre for Atomic Research, Kalpakkam-603 102, Tamil Nadu, India

E-mail : tata@igcar.ernet.in

Abstract : The availability of laser light sources and powerful low-cost computer data processing and imaging systems have helped in popularizing the confocal laser scanning microscope (CLSM) in the field of materials science and technology and in life sciences. CLSM has great advantage over a conventional microscope because it rejects light that does not come from the focal plane, enabling one to perform optical slicing and construction of three-dimensional (3D) images. Because of this unique feature, CLSM is now finding wider applications in the study of a variety of materials and process such as crystallization and glass transition in colloidal systems, phase separation in polymer blends, fracture toughness in alloys and microvisualization of corrosion. This paper reviews some of these recent applications and also discusses our results in providing evidence for long-range attraction between like-charged particles and for the occurrence of gas-solid transition in highly charged colloidal systems. Apart from colloids, other macromolecular systems (*e.g.* gels, surfactant systems, membranes *etc.*) that constitute soft matter are characterized by building blocks with typical length scales that range between tens of nanometers to micrometers. The increased dimension of these basic building blocks essentially causes the materials to be soft (*i.e.* elastic constants of the order of 10–100 dynes/cm^2) and dynamics to be very slow (~ microseconds to several seconds). The information with regard to the structure and dynamics at the lower end of length and time scales in the soft matter can be obtained using laser light scattering (photon correlation spectroscopy) and that at the higher end using CLSM. By combining judiciously the two techniques, we have investigated charged colloidal systems for their structure, dynamics and phase behavior and these results are discussed in this paper.

Keywords : Confocal microscopy, laser light scattering, colloids, gas-solid coexistence, long-range attraction

PACS Nos. : 87.64.Tt, 42.62.Fi, 64.70.Hz, 64.70.Pf, 82.70.Dd

1. Introduction

The advent of lasers and powerful low-cost computers and development of digital image processing software have paved the way for the development of single-beam confocal laser scanning microscopes. The power of CLSM lies in its ability to eliminate out-of-focus light or glare, and thus obtain three-dimensional (3D) image data from intact biological specimens by non-invasive optical sectioning. The first commercial confocal laser scanning fluorescence systems were developed in the year of 1987 by Bio-rad during the last decade the availability of confocal laser scanning microscopes of ever-increasing power and sophistication has revolutionized the science of microscopy as applied to filed of cell biology, life sciences and the materials science [1–4]. In addition to optical sectioning (images recorded as function of depth of the specimen), the ability to obtain a time series (images recorded as function of time) of 3D images from a living specimen or a colloidal sample, with temporal and spatial resolutions superior to video microscopy, has opened up new avenues of investigations previously impossible to contemplate.

Recent developments in cost effective electronic chips and fast responding detector systems along with the intense laser light sources have made the static and dynamic laser light scattering technique a versatile research tool to investigate a number of soft matter systems such as colloidal suspensions, gels, polymer solutions, surfactant systems, membranes and biological systems for characterizing their microstructure with basic building blocks having typical length scales between nanometers and micrometers particle dynamics in time scales ranging from nanoseconds to several seconds (eleven orders of magnitude). The dynamics that occurs

*Corresponding Author

in this time scale can be measured in "time-domain" using an electronic correlator designed to compute the time-correlation function [5,6]. Due to the large structural length scale, the number density of their translational degrees of freedom is many orders of magnitude smaller than that for ordinary molecular material. This and the interactions between the basic building blocks, which is typically on the order of thermal energy k_BT, implies that these materials are easily deformable by external forces [7]. For example, the shear modulus of a colloidal crystal with a lattice constant of 0.5 μm is approximately 10 dynes/cm^2, which is about 12 orders of magnitude smaller than that of atomic crystal [7–9]. Thus most of these macromolecular systems are extremely soft and can be destroyed by mechanical means very easily.

The goal of characterizing the soft matter is to understand or derive the macroscopic properties from the microscopic structure and dynamics, which essentially means characterizing the building blocks, their arrangement, motion and their internal degrees of freedom. Scattering techniques such as small-angle-X-ray scattering (SAXS), small-angle-neutron scattering (SANS) and static laser light scattering can provide information at the lower end of the length scale (~100 nm) of soft matter. The scattering techniques provide information in Fourier space and one has to apply Fourier-Transformation (FT) techniques to obtain information in real space. Multi-tau dynamic light scattering technique, also known as photon correlation spectroscopy (PCS) [5,6], which has a dynamic range of 10^{11} orders of magnitude in time starting from tens of nanoseconds helps in probing the dynamics in soft matter systems. Confocal laser scanning microscopes are found to be useful to obtain 3D structural information on the higher end of the length scale as well as dynamics at the lower-end of the time scales in the soft matter systems.

This paper describes the principles of a single-beam confocal laser-scanning microscope (CLSM) as well as laser light scattering (static and dynamic) techniques. Apart from reviewing the investigations that have been carried out using CLSM in hard-sphere and charged colloidal systems, we present our CLSM and light scattering results in highly charged colloidal systems, where CLSM is shown to be very useful tool in characterizing the inhomogeneous nature a colloidal system of highly charged particles and in establishing the existence of long-range attraction between like charged colloids. The use of CLSM in studying processes such as colloidal epitaxy, crystallization and glass transition in charged colloids is also discussed. The applications of CLSM in providing the spatial structure and coarsening dynamics of off-critical polymer mixtures undergoing phase separation, in understanding the fracture behavior and corrosion process in technological materials are also presented. Thus this paper presents the application of lasers in characterizing the microstructure and dynamics in a wide variety of hard and soft condensed matter systems.

2. Principle of confocal laser scanning microscope

Before we describe the confocal principle, it is important to know about the advantages of choosing a scanning approach, which is inherent in all confocal laser-scanning microscopes. The optical components of a conventional microscope have severe requirement as the microscope functions as parallel processing system which images the entire object field simultaneously. The scanning approach relaxes this requirement on optics as image of the entire object field is built not simultaneously but by scanning and imaging only one object point at a time. It also gives the freedom to modify the optical system in simple ways to expose the full potential of the confocal mode and many other imaging modes. The basic principle of a confocal microscope is easy to understand in spite of complicated electronic, mechanical and optical systems associated with the commercial instruments. The principle of a simple reflection mode confocal laser scanning microscope (CLSM) and a sample cell with colloidal suspension is shown in Figure 1. When a laser or any other light source illuminates a pinhole, light emerging out from the pinhole passes through a beam splitter and is focused by an objective lens to a spot in the focal plane, where the sample is placed. Light reflected from this spot is partly reflected by the beam splitter towards a pinhole in front of the detector. Light reflected from any other parts of the sample, including parts above or below the focal plane, reach the edge of the detector pinhole and will not be detected by the detector. The objective lens forms an image of the detector pinhole and the illuminating pinhole at the same spot in the focal plane, hence these are said to be confocal with each other. The selective rejection of light endows the confocal microscope with significant axial and lateral resolution. Since it rejects stray light not only from the out-of-focus specimen planes but also light scattered from within the optical instrument itself, resulting in increased contrast and signal to noise-ratio in the final image. The depth discrimination property and high quality image generation

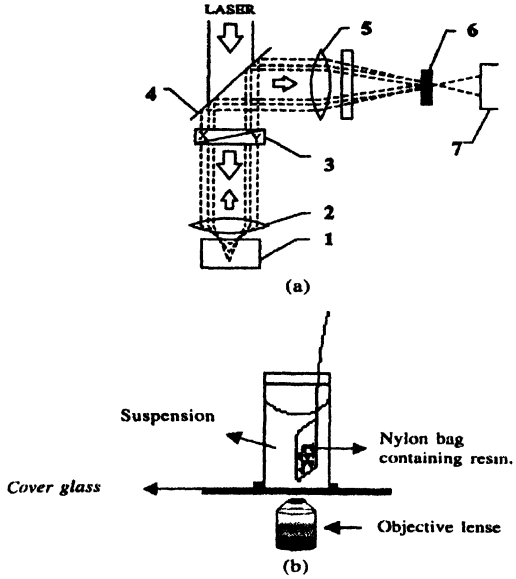

Figure 1. (a) Schematic diagram showing the principle of confocal laser scanning microscope. (1) sample, (2) objective lens, (3) XY-scanner, (4) beam splitter, (5) focusing lens, (6) pinhole and (7) detector. The depicted beam paths show that light scattered from any other position on the sample, including those above or below the focal plane, is rejected by the pinhole and (b) Schematic diagram of sample cell used for CLSM investigation.

suitable for subsequent image processing are major advantages of confocal laser scanning microscopes.

The image of certain portion of the sample using CLSM is obtained by scanning the beam using vibrating galvanometer-type mirrors or acousto-optic beam deflectors, so that the focused spot moves across the specimen. Since each point on the specimen is illuminated only for a very short time, high beam intensity is necessary. Hence, lasers have to be used as the source of light. The optical system is usually complex in scanning beam microscope (also known as scanning optical microscope (SOM)) and the magnification is coupled to the resolution; hence it is necessary to change the objective lenses in order to cover the entire magnification range. The major advantage of a SOM is that they are usually built around conventional optical microscope, which permits binocular viewing in order to locate the region of interest. Confocal laser scanning microscopes with scan speeds as high as 30 frames per second (fps) at 512 × 512-pixel resolutions are available commercially [10]. There are also tandem scanning confocal microscopes where one uses a large number of pinholes on a disk (Nipkow disc) with which the instrument acts like several hundred confocal microscopes all working in parallel [1,2]. The disk is rotated at high speed to produce a flicker-free image of the whole field of view. Great care is taken in choosing the size and spacing of the pinholes in the disk [11]. Such a tandem scanning microscopes provide a real time confocal image.

3. Laser light scattering (static and dynamic)

Consider a homodyne dynamic light scattering experiment, where one mixes scattered intensity with itself on the detector, one measures [3] the time averaged normalized intensity autocorrelation function $g^{(2)}(Q,t)$

$$g^{(2)}(Q,t) = \langle I(Q,0)I(Q,t)\rangle / \langle I(Q,0)\rangle^2 \tag{1}$$

where $I(Q,t)$ is the average scattered intensity from a suspension of N colloidal particles at a scattering wave vector $Q = |K_i - K_s| = (4\pi\mu_s/\lambda)\sin(\theta/2)$ (Figure 2(a)) and at a given time t. Here, θ is the scattering angle, μ_s is the refractive index of the dispersion medium and λ is the wavelength of laser light. $g^{(2)}(Q,t)$ is related to the normalized electric field autocorrelation function $g^{(1)}(Q,t)$ by the Siegert-Relation [5,6]

$$g^{(2)}(Q,t) = 1 + |g^{(1)}(q,t)| \tag{2}$$

As the particle positions $\{r_i(t)\}$ in a dispersion change owing to Brownian motion, the electric field $E(Q,t)$ of the light single-scattered into the far field at scattering angle θ fluctuates randomly in time. These fluctuations can be characterized using the first order electric field correlation function

$$g^{(1)}(Q,t) = \langle E(Q,0)E^*(Q,t)\rangle / \langle |E(Q,0)|^2 \rangle \tag{3}$$

which is related to the 'dynamic structure factor' or the 'intermediate scattering function' $F(Q,t)$ by

$$g^{(1)}(Q,t) = F(Q,t)/S(Q), \tag{4}$$

$$\text{where } F(Q,t) = \frac{1}{N}\sum_{i=1}^{N}\sum_{j=1}^{N}\left\langle \exp\left(iQ.(r_i(0) - r_j(t))\right)\right\rangle \tag{5}$$

and the static structure factor $S(Q) = F(Q,0)$. Information on the Brownian motion of colloidal particles is obtained from the functional dependence of $F(Q,t)$ on Q and t.

Figure 2(b) shows the schematic of our DLS set-up with a multi-tau correlator and PMT as the detector. Till 80's all the commercial instruments have employed linear correlators having 256 channels with minimum sample time τ about a microsecond. The correlation functions evaluated using a linear correlator is restricted to 256τ, hence many relaxation processes with relaxation times

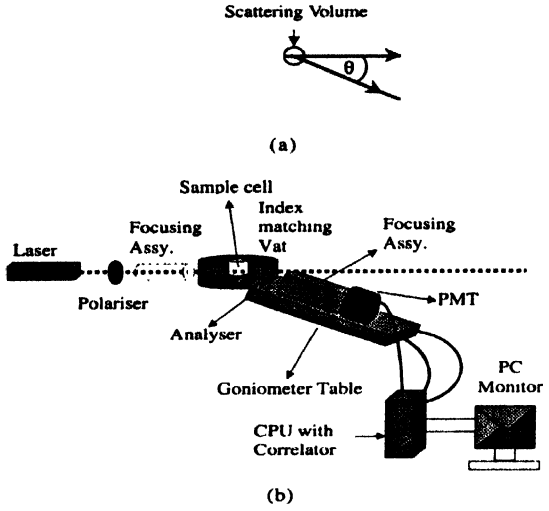

Figure 2. (a) Schematic diagram of light scattering. K_i and K_s are incident and scattered wave vectors respectively and (b) Schematic representation of our static/dynamic light scattering set-up.

extending over a wide dynamic range (~10^{10} sec), could not be studied. This lead to the development of the multiple tau correlation technique (MTC) [12] by Schatzel in the middle of 80's. The first commercial available device incorporating traditional correlation techniques as well as MTC technique was introduced in 1984 by ALV-Germany Company. With advancement of fast electronic chips and high speed PC's, there are now several manufactures supplying multiple-tau correlators, which can span a dynamic range of 10^{11} sec in time with 12 to 50 nsec as the minimum sample time. There have been some recent reports of the development of LABVIEW based software multi-tau correlators with 25ns as the sample time [13]. Charge coupled device (CCD) based dynamic light scattering system, known as multispeckle DLS set-up [14] has been developed to obtain $F(Q,t)$ at different Q-vectors simultaneously. The dynamic light scattering instrument without a correlator card serves as a static light scattering system and involves measurement of scattered intensity $I(Q)$ at different values of Q. The scattered intensity in the Rayleigh-Gans approximation is given as

$$I(Q) = CP(Q)\,S(Q), \tag{6}$$

where C is the constant [15] and the form factor $P(Q)$ for a spherical particle of radius a, is given by

$$P(Q) = 9\left[\frac{\sin(Qa) - Qa\cos(Qa)}{(Qa)^3}\right]$$

For a non-interacting colloidal suspension, $S(Q) = 1$, hence one can obtain particle size and shape by analyzing the $I(Q)$ *vs.* Q data obtained from static light scattering measurements. An interacting suspension can be characterized for its structural ordering (liquid-like, crystalline or glass-like) from the knowledge of $P(Q)$ and by analyzing the $S(Q)$.

4. Applications of CLSM in technological materials

Confocal laser scanning microscopy has found applications in processes and materials of technological importance *viz.* evaluation of the fracture process in steels [3,16] and in corrosion studies [3,17,18]. Enmark *et al* [16] have investigated the fracture behavior of surface cracked panels of tempered martensitic steels, to examine the failure conditions at temperatures corresponding to the quasi-cleavage fracture regime. Tempered martensitic steels are studied with significant interest because these being considered as structural materials for fast breeder and fusion reactors, also due to good thermo-mechanical properties and good swelling resistance to environments in fast breeder and fusion reactors. Further there is also considerable current interest with regard to characterizing the ductile-brittle transition in these materials and its significance to fracture resistance of reactor structures.

With an aim to study the fracture behavior, Enmark *et al* [16] have grown semi-elliptical surface cracks in to the center of one side of the tempered martensitic stainless steel specimens, which are rectangular in cross section. The crack creation and specimen preparation are described in detail in their original paper [16]. Samples were subjected either to tension or three point bending to achieve cracks of required dimensions. Fracture surfaces were examined using scanning election microscope and confocal laser scanning microscope. Scanning election microscopy has been used to characterize the cleavage nature of the entire fracture surface and confocal microscopy to generate quantitative, 3D topographic maps of the fracture surfaces. These maps in turn can be used with fracture reconstruction techniques to evaluate the values of crack tip opening displacement, δ^*, along the crack front at the time of the fracture. The measured δ^* values are used to calculate an effective fracture toughness for the surface cracked panels. In another study, Odette *et al* [19] have determined fracture toughness as function of test temperature for V-4Cr-4Ti alloy under both static and dynamics conditions using scanning electron microscopy and confocal microscopy. The samples used

for this study are pre-cracked specimens of small size. 3D topographies of the fracture surfaces obtained using CLSM were used along with fracture reconstruction methods to ascertain the sequence of events leading up to fracture and the critical crack tip opening at the point of crack initiation. Fracture reconstruction sequences have revealed the process of material separation in the plane of the crack as function of crack opening displacement.

Materials can fail not only due to mechanical damage leading to fracture, but also due to corrosion. Localized corrosion is known to be a major cause of degradation failure in materials of technological importance. The detection of corrosion for preventive purposes and new methods for studying the corrosion process are of great practical importance. Corrosion process can be studied using several techniques. However, the experimental methods that can (1) measure corrosion rate, (2) locate breakdown sites and (3) study the fundamental properties of passive films (such as the optical and electronic properties) and their relationship to the local stability of the films, are relatively few in number. Corrosion usually occurs locally and non-uniformly; hence experimental methods that can measure local corrosion rates accurately are as important as those that can locate the corroding sites. In order to locate corrosion site, the entire region of the corroding surface is to be imaged for which CLSM are best suited. Further these also provide information about all the three topics mentioned above.

Sukamoto *et al* [17] have demonstrated the optical slicing capability of CLSM by imaging a polycrystalline Cu substrate that has been etched preferentially with a solution of a de-aerated 0.1 M H_2SO_4 and 0.1 M H_2O_2 for 30 min. A 3D image is formed by combining a series of optical slices, where an individual optical slice represents a plane of focus. The 3D image of the etched Cu surface can be shown as fishnet plot by depth coding the section series. The depth coding procedure includes finding out the maximum intensity along the z-axis for each point in the xy-plane and converting the z-position to intensity. Alternatively xz and yz section scans are also possible. The xz and yz slice show the surface profile viewed from two perpendicular directions. In the latter mode the CLSM becomes a non-contact surface profilometer. This surface profiling technique can also be used to produce one and 2D plots of surface topography with a sensitivity of better than 100 nm. Further, the soft ware of CLSM can provide 3D projections of the series of optical sections. This allows characterizing the pores in a porous material or micro-pits on the surface of a corroded material.

Corrosion of cooling system materials is known to be due to sulphate reducing bacteria (SRB) [18] and study of SRB induced corrosion of titanium is of current interest because of its increased use in industrial cooling systems. Recently, Rao *et al* [18] have carried out a detailed study on pitting corrosion of titanium by exposing specimens to SRB (*Desulfovibrio vulgaris*) culture for 90 days under controlled conditions. These specimens were examined using our CLSM (Model : Leica TCS SP2 RS, laser source Argon 100 mW, wavelength 488 nm). Figure 3 shows pitting corrosion of titanium specimen exposed to SRB culture. The area of the specimen scanned was 250 × 250 μm using 40x objective. The control set of titanium coupons (*i.e.* coupons exposed to sterilized SRB medium) did not show any pitting corrosion, clearly indicating that pitting corrosion occurs due to the SRB

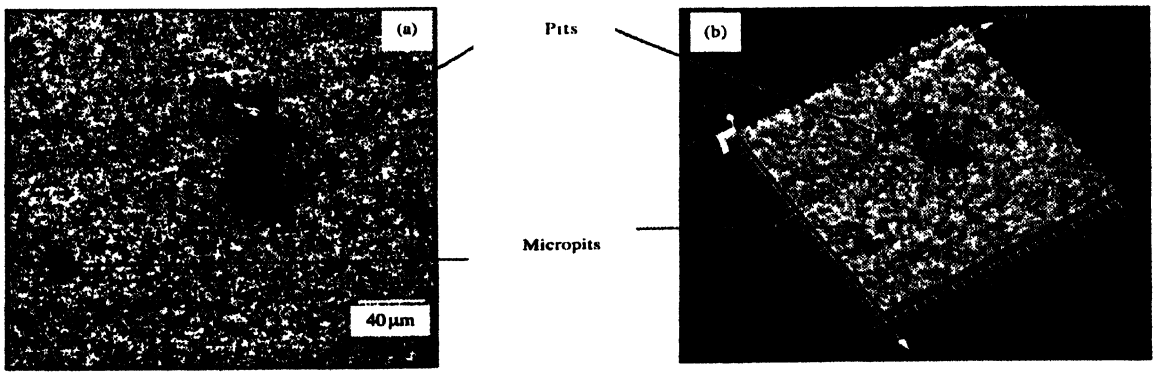

Figure 3. (a) CLSM image (optical slice) of the titanium coupon exposed to SRB culture showing pits and micropits and (b) Reconstructed 3D image using 25 optical slices at a z-separation of 1 µm showing pits of size 50–60 µm extending up to a depth of more than 25 µm and micropits of size 5–10 µm.

and their microbiological activity at the metal/bio-film interface.

SRB form a biofilm having a crevice like geometry on the metal surface. Further the bacteria produce hydrogen sulphide (H_2S) as well as phosphine (PH_3). H_2S thus produced is a reducing agent and also inhibits the growth of most aerobic bacteria. Microbial colonization promotes a decrease in the passive film (TiO_2-film) resistance by producing acidic metabolites and complexing substances [18]. The rapid decay of the passive film favors the initiation of localized corrosion process such as pitting. CLSM has thus helped us to provide evidence for pitting corrosion of titanium in the form of 3D images of micropits caused by SRB.

5. Applications of CLSM and laser light scattering in soft condensed matter

Confocal laser scanning microscopy and laser light scattering techniques have been extensively used to probe the structure, dynamics and phase separation phenomenon in a variety of soft matter systems. Here we present the application of these techniques in characterizing structural ordering and dynamics in colloidal crystals [15,20,21], colloidal glasses [4,22], gas-solid transition [4] in highly charged colloids and also in determining the pair-potential between like-charged colloids. The applications of CLSM in studying process such as colloidal Epitaxy and coarsening dynamics of off critical polymer mixture undergoing phase separation are also discussed.

5.1. Colloidal glass transition and dynamical heterogeneities in hard-sphere systems :

Glassy phase can be obtained by abruptly cooling (quenching) and/or compressing (pressure crush) a liquid. Many liquids undergoing glass transition exhibit nonexponential decay of time correlation functions and non-Arrehenius temperature dependence of relaxation time with decreasing temperature [23]. In the recent past researchers have focused their attention on nonexponential relaxation by performing computer simulations [24] and experiments [25] on atomic systems. These studies suggest that a superposition of different relaxation processes or dynamical heterogeneity underlies the nonexponential behavior. The direct experimental evidence for the existence of dynamical heterogeneities has come only recently from studies on HS colloidal suspensions [22]. This is because colloidal particles can be observed under CLSM and the time series of digital images of the colloidal particles in optical slices in the bulk of the sample enables one to monitor the motion of the particles. Evidence for the presence of dynamical heterogeneities in dense colloidal liquids and colloidal glasses were obtained from the analysis of particle trajectories. CLSM studies were carried out on hard-sphere suspensions of PMMA particles with fluorescent dye. Fluorescence confocal laser scanning microscopy has been used to record the particle trajectories in samples with ϕ in the range of 0.46–0.64. Glass transition was observed to occur at a volume fraction of $\phi \sim 0.57$. Using the positions of centers of the spheres recorded over several time steps, one obtains several quantities such as particle displacements Δx in a time interval τ, mean square displacement (MSD) $\langle x^2(t)\rangle$, non-Gaussian parameter $\alpha_2(\tau)$ defined as

$$\alpha_2(\tau) = \frac{\langle \Delta x^4(\tau) \rangle}{3 \langle \Delta x^2 \rangle^2} - 1, \tag{8}$$

self-part of the van-Hove correlation function $G_s(x,\tau)$ [22,26] and pair-correlation function $g(r)$.

Dynamical heterogeneities near a glass transition can be detected by investigating time dependence of $G_s(x,t)$. To a first approximation $G_s(x,t)$ has a Gaussian form, but deviation from this at intermediate times reflect the presence of dynamical heterogeneities [22,26]. Such deviations can be characterized by $\alpha_2(t)$. $\alpha_2(t) = 0$ if $G_s(x,t)$ is a Gaussian. $\alpha_2(t)_{as}$ function of time exhibits a peak and the peak value of $\alpha_2(t)$ increases as one approach the glass transition. The time t^* at which $\alpha_2(t)$ attains the peak is found to increase with increase in ϕ. The increase in $\alpha_2(t)$ is an evidence that the dynamics of the colloidal liquid becomes more heterogeneous with increasing ϕ. In order to study the structural relaxation and cooperative motion of particles in the super cooled fluid, fastest (mobile) particles are identified by selecting particles which have undergone displacements greater than a cut of distance r^* in the time interval $[0,t^*]$. This definition implies that mobile particles are those that contribute to the long tail of $G_s(x,t^*)$. For the super cooled fluid, the mobile particles were strongly correlated and form extended clusters [22,26]. These observations provide (a) direct evidence for existence of dynamical heterogeneities in super cooled liquids and (b) that α-relaxation in super cooled fluids occur by means of cooperative particle motion *viz.* when one particle moves another particle moves by closely following the first. The cluster size is found to increase dramatically as ϕ is increased. Constant pressure simulations by Tata *et al* [26] as function of osmotic pressure for charged colloids have also shown

existence of dynamical heterogeneities near the glass transition brought out by sudden application of pressure. These observations thus provide support in favor of Adams and Gibbs approach [27] to the theory of glass transition. Apart form providing direct evidence for the existence of dynamical heterogeneities in super cooled fluids near colloidal glass transition, confocal laser scanning microscopy also has been used to study the properties of cage rearrangements near the colloidal glass transition [22], thus providing direct visualization of structural relaxation in a super cooled state.

5.2. Laser light scattering studies on charged colloidal crystals :

Hard-sphere colloids freeze into a face centered cubic structure (fcc) for $\phi > 0.48$ and into a glass-like order for $\phi > 0.57$. Volume fraction is the only variable for driving the order-disorder transition hard-sphere colloids. However, charge stabilized colloids, also known as charged colloids, interact predominantly *via* repulsive screened Coulomb interaction [8,9] and its range and strength is tunable over a wide range by varying the suspension parameters such as volume fraction ϕ, salt concentration C_s, and charge density σ on the particle. Charged colloids freeze in to a body centered cubic (bcc) structure at low volume fraction (typically $\phi < 0.1$) and to an FCC structure at higher values of ϕ [8,9]. Colloidal crystals exhibit iridescence due to Bragg diffraction of visible light and their structure and dynamics can be investigated using static and dynamic light scattering techniques (DLS) [8,9]. These crystals differ from the atomic crystals not only in particle size and lattice constants but also in dynamics due to the hydrodynamic interaction by the intervening solvent fluid. Hydrodynamic interaction between colloidal particles arises when the moving particles exchange momentum through the viscous fluid [28]. The fluid causes friction, which strongly dampens the lattice vibrations [28,29]. The theory of hydrodynamic interactions in charged colloidal crystals [28] predicts that the damping of transverse modes vanishes in the long-wavelength (i.e. wave number $q = 0$) limit. All the other modes are predicted to be overdamped due to the strong frictional forces [28,29]. At small wave numbers there is no relative motion of colloidal particles and the fluid. Hence the overdamped transverse modes turn propagative, as q tends to zero [28,29]. So far, this prediction of hydrodynamic theory of charged colloidal crystals has not been observed experimentally and also the volume fraction dependence of this transition is not examined either theoretically or experimentally.

All previous experiments of phonon dispersion measurements in charged colloidal crystals were carried out on dilute ($\phi \approx 0.002$–0.005) aqueous suspensions of polystyrene particles confined in a thin (~30–130 μm) cell [28,29] to prevent multiple scattering of light. However, the transition of transverse modes turning from overdamped to propagative was not observed in these measurements due to small size of the crystallites. We have grown large (~3 mm size) colloidal crystals of silica particles (diameter d = 120 nm) dispersed in 90 : 10 ethylene glycol-water (EGW) mixture, which are free from multiple scattering of light [20]. Dynamic light scattering measurements were carried out at room temperature on two samples S1 and S2 having volume fractions 0.048 and 0.064 respectively. The corresponding lattice constants of samples S1 and S2 estimated from static laser light scattering measurements (Figure 4) are R_0 = 335 nm and 302 nm respectively. R_0 is calculated using the relations $R_0 = 2\sqrt{2}\pi/k_{110}$ and $R_0 = d(\pi/3\phi)^{1/3}$. k_{110} is the first Bragg peak position in $I(k)$ *vs.* k plot (Figure 4). The insets in Figure 4 show photographs of samples S1 and S2 having large size (about 3 mm) single crystals exhibiting iridescence under white light illumination.

The phonon dispersion curves (Figure 5) [20] are obtained from dynamic light scattering measurements. Our laser light scattering system consists of a (Ar + Kr) mixed-ion laser, and a 50 mW He-Ne laser, Malvern (UK) 4700 multi-tau correlator and a goniometer, with

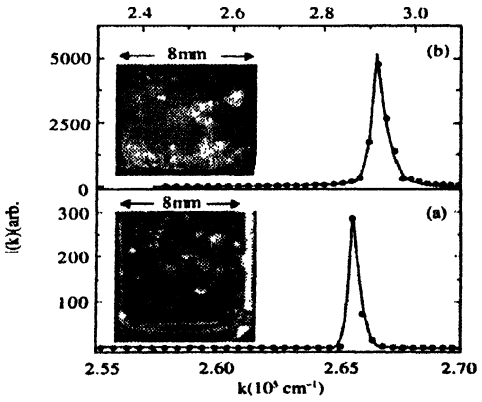

Figure 4. Scattered intensity $I(k)$ *vs.* scattering wavevector k from crystallites at the center of the cell, whose (110) planes are oriented perpendicular to the scattering plane (xy-plane). (a) In sample S1, (110) Bragg peak occurs at $k = 2.656 \times 10^5$ cm^{-1} and (b) in sample S2 Bragg peak occurs at $k = 2.918 \times 10^5$ cm^{-1}.

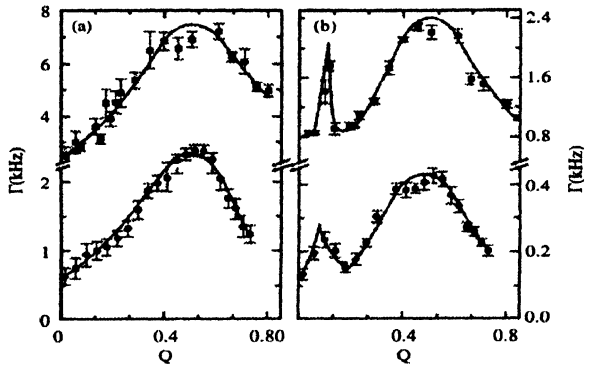

Figure 5. Measured phonon dispersion curves along [110] direction of colloidal single crystals of 3 mm size and having bcc structure. (a) Longitudinal and (b) transverse. Filled circles and filled squares correspond to dispersion in crystals with $\phi = 0.048$ and 0.064. The lines are guide to the eye. Note that the transverse mode turns propagative at $Q \approx 0.076$ in a crystal with $\phi = 0.048$ and at $Q \approx 0.11$ in a crystal with $\phi = 0.064$.

photomultiplier tube as the detector. The decay rates Γ of longitudinal and transverse lattice modes are obtained by subjecting $g^{(1)}(k,t)$ to mixed mode analysis using nonlinear-least square fit method. The measured transverse modes, apart from exhibiting the expected dispersion away from small Q-regime, where $Q = qR_0/(2\sqrt{2}\pi)$ is the reduced wave number, also show a sharp peak at $Q \approx 0.076$ in a crystal with $\phi = 0.048$ and at $Q \approx 0.11$ in a crystal with $\phi = 0.064$. The observation of sharp peaks constitutes an unambiguous evidence for the transition of the overdamped transverse modes to propagating modes as predicted by the hydrodynamic theory of charged colloidal crystals [20].

5.3. Gas-solid coexistence in charged colloids :

Effective surface charge (Ze) or effective charge density σ ($= Ze/\pi d^2$) of the colloidal particle plays an important role in determining the structural order and the phase behavior of charged colloids. When Ze is quite high, the corresponding counterion concentration (n_pZ, where n_p is the particle concentration) is also high as compared to the salt ion concentration. Under these conditions, deionized suspensions are expected to remain inhomogeneous in the form of a gas-solid coexistence.

Tata *et al* [30] have synthesized highly charged polychlorostyrene styrene sulfonate (PCS) particles in aqueous medium. The particles have a diameter d of 180 nm and an effective charge density $\sigma = 0.25$ μC/cm^2. These suspensions are turbid for performing light scattering studies. However, they have sufficient electron density difference (contrast) for characterizing their structure using ultra-small-angle-X-ray-scattering (USAXS) [26]. USAXS profiles have revealed glass-like ordering and non-space filling nature of these suspensions. Confocal laser scanning microscopic study on these samples showed the presence of large size voids deep inside the suspensions, which coexisted, with disordered dense regions of particles [8,9,30]. The voids are found to have only a few colloidal particles. Averaging of the image frames over several seconds improved the sharpness of the image, which suggests that the disordered dense regions are amorphous. The split-second peak in the structure factor measured using USAXS apparatus also confirmed the glass-like structure within the dense regions [9,30]. The observation of amorphous dense phase together with voids provides an evidence for the gas-solid coexistence and hence suggests existence of long-range attraction in the interparticle interaction of charged colloids.

Recently, Yamanaka *et al* [31] and Toyotama *et al* [32] have reported that initially a homogeneous disordered (liquid-like ordered) suspension undergoes crystallization upon increasing the effective charge density σ on the particles. This crystalline order (solid phase) is found to disorder once gain on further increase of σ. These observations are understood by performing Monte Carlo (MC) simulations [33] using Sogami-Ise pair-potential $U(r)$, which has a long-range attractive term in addition to the screened Coulomb repulsive term. These simulations showed existence of a homogenous ordered phase in a narrow range of σ whereas the solid (crystalline) region observed by Yamanaka *et al* [31] and Toyotama *et al* [32] exists at a relatively higher range of σ. At these values of σ, simulations showed coexistence of ordered structure with voids. However, the experimental observation of solid region is completely based on iridescence from samples and detailed investigations to characterize the structure and for the inhomogeneous nature of the suspension was not carried out. These results have motivated us to carry out systematic light scattering and CLSM studies on deionized aqueous suspensions of polystyrene particles with different size and different charge densities. Table 1 summarizes the sample details of small size (SS) suitable for laser light scattering studies as well as large size (LS) particles suitable for confocal microscopy studies. In order to minimize the effect of gravity all these samples have been prepared under density-matched conditions by dispersing the particles in 50 : 50 (H_2O + D_2O) mixture.

Figure 6 shows the photographs of samples SS1, SS3 and SS5, which are arranged in increasing σ. Samples

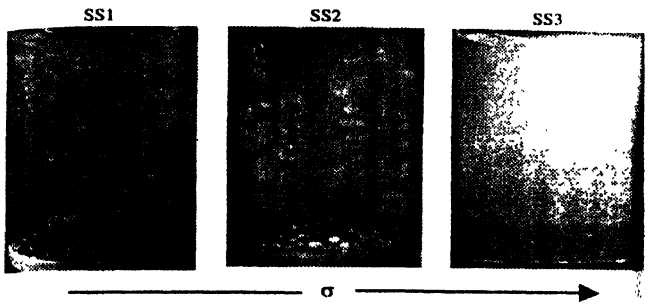

Figure 6. Photographs of the samples S1, S3 and S5 arranged in increasing charge density σ. Sample SS1 and SS3 show iridescence, whereas no iridescence is observed in sample SS5. Mixed bed ion exchange resins, which remove ionic impurities in the suspension, can be seen at the bottom of the cells.

SS1-SS3 showed iridescence over the entire volume of the cell (Figure 6) indicating the suspensions are crystallized, where as sample SS4 and SS5 did not exhibit iridescence. The structure factor $S(k)$ measured as function of scattering wavevector k (Figure 7) revealed that crystalline order in the both samples is bcc. However the (110)-peak peak position was found to shift to higher k-side. The volume fraction ϕ_d estimated from the (110)-peak position, k_{max} using the relation

Table 1. Sample details of aqueous suspensions of polystyrene particles.

Sample No.	d(nm)	$\sigma(\mu C/cm^2)$	ϕ
SS0	136	0.24	0.0005
SS1	136	0.24	0.001
SS2	104	0.41	0.001
SS3	104	0.41	0.005
SS4	126	0.512	0.001
SS5	126	0.512	0.005
LS1	486	4.57	0.005
LS2	486	4.57	0.030
LS3	378	25.8	0.005

$$\phi = \frac{\pi d^3}{\sqrt{2}} \cdot \frac{1}{2\pi} \left| \frac{k_{max}}{2\pi} \right. \tag{9}$$

is found to be higher than ϕ_0, where ϕ_0 is the volume fraction of the homogenous suspension determined independently by drying a known amount of deionized suspension. This implies that samples SS1 and SS3 are inhomogeneous (*i.e.* the ordered phase does not occupy the full volume). The fraction of the volume that is not occupied by the ordered region is expected to appear as particle free regions (voids). Because of significant multiple scattering, we failed to measure $S(k)$ in samples SS4 and SS5 using light scattering. Since the charge

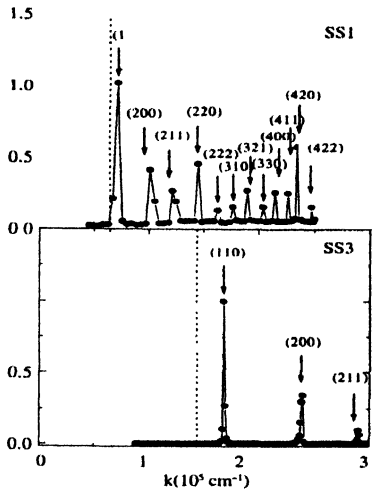

Figure 7. $S(k)$ as a function of k measured in samples SS1 and SS3. The vertical dotted line shows the position of k calculated from the eq. (9).

density of particles of SS4 and SS5 are higher than that of SS1-SS3, we expect these samples also to be inhomogeneous and disordered because they did not exhibit iridescence.

In order to know whether voids exit in these samples or not, we have carried out CLSM studies by transferring these samples into another cylindrical quartz cells with a cover slip glued at the bottom of the cell (Figure 1b). Clean nylon bags containing the mixed-bed ion exchange resins were hung from the top of the cell and sealed hermetically with a glass plate and a Parafilm. CLSM allows one to image deep inside the suspension. Figure 8 shows the coexistence of crystallites with voids inside the suspension at a depth of 55μm from the cover slip. Reconstructed 3D image (Figure 8b) shows that voids extend up to a depth of ~40 μm. CLSM observations confirm the inhomogeneous nature of suspensions as revealed by light scattering measurements. Thus, confocal microscopy together with light scattering has helped to characterize the inhomogeneous nature of the crystalline order in suspensions of relatively small size particles with intermediate particle charge density. The void fraction $V_f = [1 - (\phi/\phi_d)]$ for samples SS1, SS2 and SS3 estimated from light scattering studies is 0.27, 0.47 and 0.36, respectively [34] and ϕ_d is the volume fraction of the ordered (dense) phase. Figure 9 shows the CLSM image of the sample SS5 taken at a depth of 70 μm from the cover slip. From the image, it can be seen that the voids coexist with dense phase which is disordered. The disorder within the dense phase is characterized to be glass-like

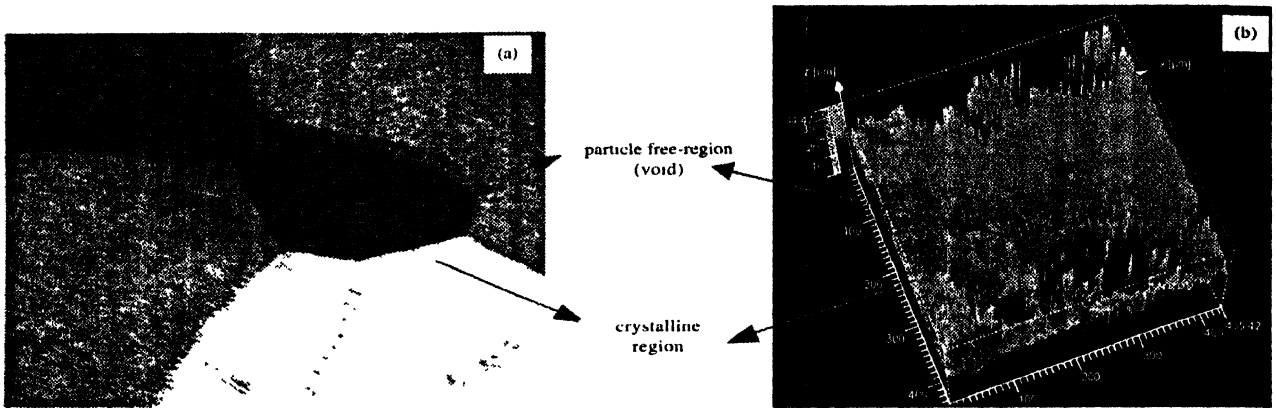

Figure 8. (a) CLSM micrograph averaged over 20 frames showing voids (black regions) with ordered regions (white regions) for sample SS3 using λ = 488 nm of Ar-ion laser and 40x/0.75 objective. Scale bar = 20 μm and (b) 3D-reconstructued CLSM image (size 435 × 435 × 35 μm^3) from 20 such optical slices revealing coexistence of voids with ordered regions.

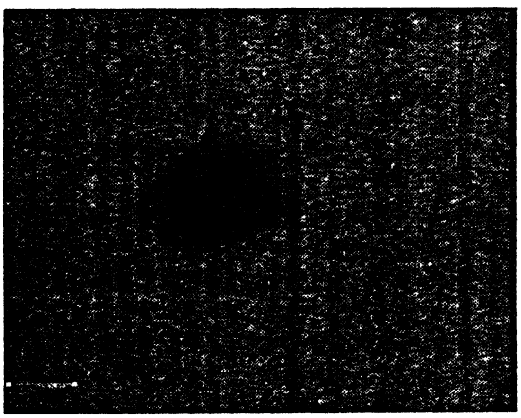

Figure 9. CLSM micrograph averaged over 20 frames and taken at distance of 70 μm from cover glass, showing voids (black regions) with disordered regions (white regions) for sample SS5 using λ = 488 nm of Ar-ion laser and 40x/0.75 objective. Scale bar = 20 μm.

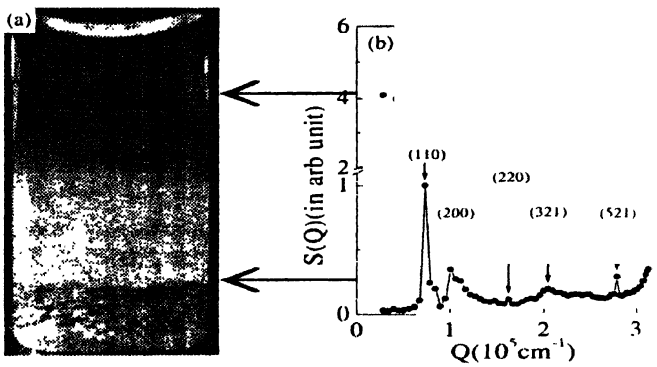

Figure 10. (a) Photograph of the sample SS0 (ϕ = 0.0005) exhibiting macroscopic phase separation in the form of dense phase showing iridescence (at the bottom) coexists with a rare phase (at the top) and (b) $S(k)$ *vs.* k measured in the rare phase (top curve) shows gas-like disorder and that measured in the dense phase (bottom curve) show bcc crystalline order.

(amorphous) by performing averaging over frames. If the disorder is solid-like the image obtained by frame averaging is expected to be much sharper than a single image. We found that CLSM image obtained by averaging over 20 frames has improved the sharpness of the image, which suggests that the dense disordered regions are glass-like (amorphous) [34]. In case of very dilute samples such as SS0, the voids constitute the majority phase leading to macroscopic phase separation. Indeed sample SS0 exhibited macroscopic phase separation (Figure 10a) in the form of dense phase at the bottom of cell having iridescence and a rare phase at the top. $S(Q)$ measured in the top and bottom regions revealed respectively that the rare phase is gas-like disordered and dense phase (Figure 10b) consists of crystallites with bcc ordering.

Structural ordering and the phase behavior as function of ϕ in suspension of *large* size particles (d = 486 nm and 378 nm) have been characterized using CLSM. Table 1 summarizes the sample details used for the CLSM investigations. Samples LS1 and LS3 have same ϕ but differ widely in σ. LS1 is found to exhibit macro-phase separation (Figure 11A) in the form of a dense phase at the bottom and a rare phase at the top of the cell. The dense phase is identified to be crystalline as it exhibits iridescence (Figure 11C) and the rare phase to be gas-like as it is very dilute. Samples with volume fractions above 0.01 did not show macro-phase separation but found to have a coexistence of ordered regions with voids (Figure 12A). Sample LS3 is with high charge density particles and did not exhibit either macroscopic phase separation or iridescence (Figure 11B). CLSM

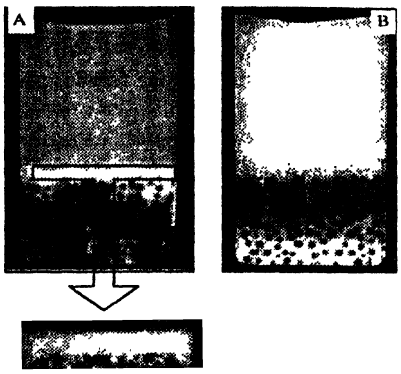

Figure 11. (A) Photograph of sample LS1 with a volume fraction of 0.005 exhibits macroscopic phase separation (gas-solid coexistence) in the form of dense phase (white regions just above the ion-exchange resins). The dense phase is crystalline as it exhibits iridescence and its magnified high-resolution digital image is shown in Figure (C). Sample LS3 (Figure (B)) is of high charge density particles with volume fraction same as LS1 but exhibits neither macroscopic phase separation nor iridescence.

investigations on this sample showed voids coexisting with disordered regions (Figure 12B). The disordered structure is identified to be glass-like (amorphous) from the increased sharpness of time-averaged images [3]. Thus, our studies on suspensions of highly charged particles (small as well as large) confirm the occurrence of gas-solid transition.

The occurrence of gas-solid transition in highly charged colloids suggest the existence of long-range attraction in the effective pair-potential $U(r)$ of like charged particles [3,33]. MC simulations as a function of σ using Sogami-Ise pair-potential $U(r)$ have shown gas-solid coexistence in the form of voids with ordered regions at intermediate charge densities and voids with glass-like disordered at higher charge densities [33]. When the charge density of the particles is high, the

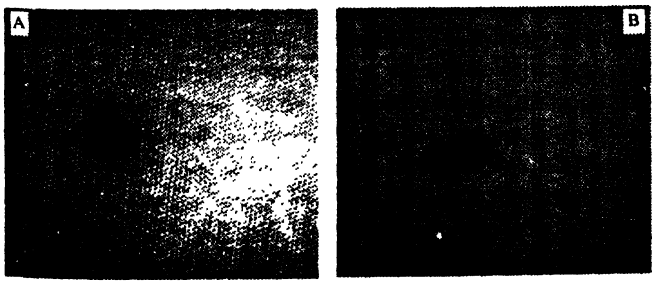

Figure 12. CLSM micrographs showing coexistence of (A) ordered region with voids in sample LS2 and (B) disordered region with voids in sample LS3. Micrograph A corresponds to 16 frames average using 20x/0.5 objective at z-distance of 30 μm from cover glass. Micrograph (B) corresponds to 8 frames average using 40x/1.2 objective at z-distance of 39.5 μm from cover glass.

corresponding well depth U_m of $U(r)$ is quite large ($> k_BT$) and the well position R_m is also less than the average interparticle separation R_0 [33]. Hence, the particles experience strong attractive forces arising from the large well depths leading to the formation of ordered or disordered dense regions coexisting with voids.

Occurrence of gas-solid transition and gas-liquid transition [35] in charged colloids can also be understood using 'volume term theories' [36]. However, recent calculations [37] based on Poisson-Boltzmann (PB) cell model, have clearly shown that the prediction of spinodal instability by volume term theory, which is responsible for gas-solid and gas-liquid transitions in charged colloids, is spurious and arises due to linearization of PB equation. The PB cell model shows that the nonlinear PB calculations did not show any spinodal instability [37].

5.4. Evidence for long-range attraction between like-charged colloidal particles :

The observations such as vapor-liquid condensation [9,35], reentrant transition as function of C_s [9,35] and σ [33,34] and existence of metastable colloidal crystals [38] lead to a debate about the existence of long-range attractive term in the interparticle interaction of these suspensions. This has renewed interest in investigating the pair-potential both theoretically as well as experimentally [9,39-41]. Recent measurements of $U(r)$ on very dilute charged colloids confined between charged plates using digital video microscopy (DVM) have shown existence of long-range attraction in $U(r)$ for the plate separation below a certain value and pure repulsion beyond this separation [40]. These experiments led to the belief that attraction between like-charged colloids arise due to many body effects, whereas $U(r)$ is repulsive [40,41].

In order to verify whether there exists an attractive term in the pair-potential between like-charged colloids, detailed confocal microscopy studies have been carried out on highly charged deionized latex suspensions of polystyrene particles having a diameter d = 600 nm and surface charge density σ = 2.7μC/cm^2. At very low volume fraction (ϕ = 0.0001), the many body interactions will be completely absent and effective interaction is truly pair-potential and hence, it can be obtained using the relation [9,40]

$$g(r) = \exp\left(U(r)/k_BT\right). \tag{10}$$

The pair-correlation function $g(r)$ is calculated using the particle coordinates. The experiment involves generating several thousands of images of particles and

obtaining particle coordinates by image analysis. The $U(r)$ thus obtained should correspond to only interaction between particles and should not be influenced by walls of the sample container. Hence, images should be recorded far away from the walls. This can only be done using CLSM as it can probe deep inside the suspension.

Typical confocal images of particles in a suspension with $\phi = 0.0001$, recorded at a distance of 600 μm from cover glass, is shown in Figures 13 (a and b). Figure 13c shows the pair-correlation function $g(r)$ calculated using particle positions obtained from 4500 such images taken at different depths and at different times. The corresponding $U(r)$ obtained using eq. 10 is shown as Figure 13d. Existence of a single peak in $g(r)$ indicates that the suspension is gas-like disordered and existence of pairs with an interparticle distance of 1.5 μm. U(r) shows an attractive minimum, U_m at an interparticle distance of 1.5 μm. Since $U_m > k_BT$, one is expected to observe bound pairs due to strong attraction, which is long-ranged (R_m = 1.5 μm). Image shown in Figure 13a clearly shows existence of several such bound pairs [42]. These pairs are found to be stable over several seconds. Three and four-particle clusters (Figure 13b), which are a few in number also have been observed. Occasionally clusters as well as bound pairs are found to exchange particles. These observations provide a direct evidence

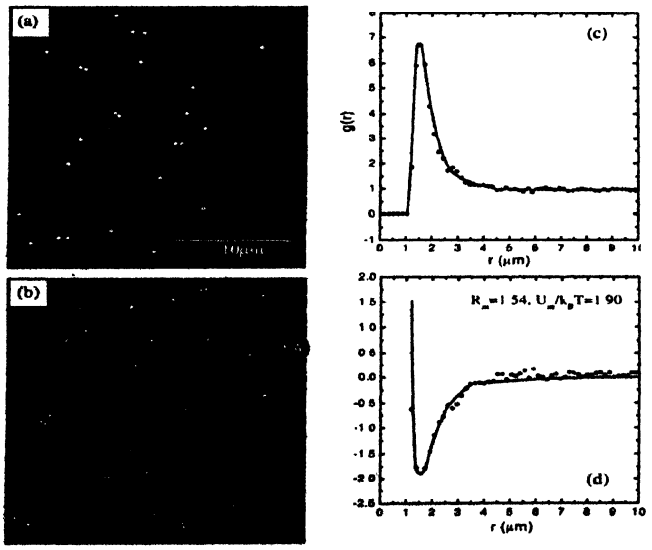

Figure 13. CLSM images (a) showing bound pairs (marked by arrows), (b) showing two three particle clusters (marked by arrows) and four and five particle clusters (marked by circles). Images are recorded using 40x/0.75 objective using 488 nm laser line of Ar-ion laser, (c) Pair-correlation function $g(r)$ *vs.* interparticle distance r calculated using 4500 image frames and (d) Pair-potential $U(r)$ *vs.* r calculated from $g(r)$ using eq. (10).

for existence of long-range attraction between like-charged colloids [42]. Further, the effective pair-potential $U(r)$ between like-charged colloids is found to have long-range attractive term [42].

5.5. Colloidal epitaxy :

As mentioned earlier, the colloidal crystals are 3D periodic structures with lattice constants of the order of microns and have many technological applications. Such applications require large single crystals with adjustable crystal orientation. Van Blaaderen *et al* have recently developed a 'colloidal epitaxy process' [43] similar to that employed for epitaxial growth of thin atomic crystalline layers on a template consisting of an oriented single crystal. This is also known as template-directed crystallization. A 500 nm-thick fluorescent polymer layer with holes made with electron beam lithography has been used as a template. The thickness is close to the particle radius (525 nm) of the fluorescent silica spheres. The interparticle forces are made hard-sphere-like by properly choosing the dispersion medium and the ionic strength of the suspension. Controlled layer-by-layer growth was achieved by slow sedimentation of the particles on to the substrate. By preparing a pattern of holes matching with the (100) plane of fcc crystal, a pure crystal of several millimeters of thickness was formed. The three dimensional stack of confocal micrographs obtained using a fluorescence confocal laser scanning microscope has been analyzed to characterize the structure and stacking of the crystal structure. The single crystal grown on (100) is found to be fcc. The structures grown on (110) plane are found to be less dense and have no twinning directions. It is shown that creating an intentional lattice mismatch can grow different defect structures. The manipulative capabilities of colloidal epitaxy are also demonstrated by making simple change in the lattice spacing between two adjacent (100) planes. Fluorescence confocal microscopy is shown to be of immense use in determining symmetry of the layers, the defect structure resulting from intentional mismatch of the lattice spacing and the crystal structure of the large size colloidal crystals, grown using template directed colloidal crystallization.

A variety of colloidal crystal structures in hard sphere as well as charged colloids have been grown using colloidal epitaxy process and confocal microscopy has been employed to characterize the 3D structure. For example colloidal epitaxy process has been used to grow

HS colloidal crystal of stacking fault free fcc structure using templates with unique, non-twinning (100) [43] or (110) [44] fcc crystal plane symmetry. Hoogenboom *et al* [45] have used one-dimensional (1D) pattern of lines that has a surface charge similar to that of charged colloids was used as template. Since charged colloids interact through long-range interaction, it is possible to grow 3D crystals even with 1D template. Whereas 3D crystal growth using 1D template was found unsuccessful in case of colloids with short-range attraction. At volume fraction where the bulk behavior in charged colloids leads to bcc crystallization, the 1D template was found to induce formation of a metastable fcc crystal. They have also investigated in detail the effect of template spacing on epitaxially grown charged colloidal crystals.

5.6. Characterization of phase separation in polymer mixtures :

If a binary mixture of two chemical components, which is homogeneous at high temperature and exhibits phase separation upon cooling below a composition-dependent coexistence temperature $T_c(\phi)$, is rapidly cooled from the single phase region to a temperature below the coexistence curve, but above the spinodal decomposition curve $T_s(\phi)$, the mixture is unstable, and rapidly separates into two spatially discontinuous phases [46]. In the case of nucleation and growth regime, the minority phase droplets are quite polydisperse and can have complicated morphologies. Hence it is difficult to interpret the data from scattering experiments. The conventional microscopes are inadequate to probe this regime as their large depth of field limits them. Confocal microscopy is shown to provide answers to many questions regarding the spatial structure and coarsening dynamics of off-critical mixtures undergoing phase separation [46,47].

Using CLSM, White and Wiltzius [46] have determined domain size distributions and spatial correlation at various coarsening times in samples with low minority phase volume fractions ($0.021 < \phi < 0.067$). The studied mixtures consisted of low molecular weight, low polydispersity oligomers of polystyrene (PS) and polybutadiene (PB). Very small quantity of fluorescent dye, Pyrromethene 580 was used to provide contrast between the phases. Both PB-rich and PS-rich mixtures have been studied. All the PS-rich samples had 75% PS by volume and the minority phase volume fractions being ϕ = 0.067, 0.040 and 0.021. The samples were allowed to coarsen for specified times (20 to 320 hours) at the chosen quench temperature, and then frozen for imaging with a second quench to room temperature. 30–50 optical sections separated in depth by a distance of 0.3 μm, with a lateral resolution of approximately 0.3 μm are acquired using fluorescent CLSM, which allowed constructing 3D images of micron size features. These binary images have been used for determining the size and location of each of the minority phase domains, as well as the overall minority phase volume fraction of the sample. Using this computer analysis White and Wiltzius [46] have calculated $F(R,t)$, the distribution of domain radii R, at coarsening times t from different PS-rich samples and also the pair-correlation function $G(r,t)$. Quantitative analysis of CLSM data revealed that in polymer mixtures with moderately low volume fractions, the coarsening occurs almost entirely by domain coalescence.

Apart from the study of nucleation and growth regime, confocal laser scanning microscopy has also found application in the investigation of polymer mixtures quenched to the spinodal region of the phase diagram [47]. When a polymer mixture is rapidly quenched to the spinodal region, the unstable mixture separates *via* spinodal decomposition into two phases and forms a bicontinuous two-phase structure, if the volume fraction of one of the phases is close to 0.5. In the past several studies, using scattering techniques, have concentrated on understanding the dynamics of spinodal decomposition including the time evolution of structural properties such as characteristic wavelength, Λ_m of the phase-separated structure. However not many studies exist to estimate the Gaussian curvature of interfaces in polymer blends, microemulsions and other complex fluids. The Gaussian curvature K and the mean curvature H are two interfacial curvatures, which characterize an interface. Since the curvatures of the surface vary from point to point, it is better to define the area averaged mean curvature, $\langle H \rangle$, and Gaussian curvature $\langle K \rangle$ [47],

$$\langle H \rangle = \frac{1}{2}\frac{\iint (k_1 + k_2)da}{\iint da}, \langle K \rangle = \frac{1}{2}\frac{\iint (k_1 k_2)da}{\iint da}, \quad (11)$$

where da is the area element of the interface and k_1, k_2 are the principal curvatures of the interface at point of interest.

Though scattering techniques yield information on mean curvature H, the determination of Gaussian curvature K is still found to be difficult because of large experimental errors associated with these measurements. However recently Jinnai *et al* [47] have shown that

confocal laser-scanning microscopy provides direct measurement of both the curvatures with sufficient accuracy. For this study, Jinnai *et al* have used a polymer blend consisted of 50/50 wt% of polybutadiene and poly (styrene-ran-butadiene). Anthracene was attached to PB for contrast enhancement. These experimental studies demonstrate the importance of confocal laser scanning microscopy in obtaining a quantitative understanding of complex phenomenon such as phase separation in polymer mixtures.

6. Conclusions

Conventional optical microscopy with digital video imaging technique provides only 2D information. On the other hand, confocal laser scanning microscopy has depth discrimination property, which allows one to image the volume of a specimen. Since the images are acquired by scanning and the image data is available in digital form, the data can be subjected to image enhancement and processing techniques without the loss of resolution. Since CLSM provides high-resolution digital images, the 3D image data can be subjected to quantitative analysis. Since one does not need to destroy the specimens, confocal microscope serves as a non-destructive three-dimensional probe.

Confocal microscopes are found to have applications in studying fracture process in martensitic steels and alloys which are very promising candidates for structural applications in reactors. One can generate quantitative, 3D topographic maps of the fracture surfaces. Fracture reconstruction sequences analyzed together with these maps allow one to evaluate the values of crack tip opening displacement along the crack front at the time of fracture, which can be compared with finite element calculations. Such measurements and comparison with calculations have been shown to throw more light in understanding the fracture process. The failure of structural components can happen not only due to the mechanical damage but also due to corrosion, which usually occurs locally and non-uniformly. Controlling corrosion has major financial impact on industry. Titanium, an important structural material used in industrial cooling systems, is known to exhibit corrosion resistance by virtue of its tenacious oxide film. Confocal microscopy studies on titanium exposed to the sulphate reducing bacteria (SRB) culture has provided insight into the failure of TiO_2 film leading to pitting corrosion of titanium. Since CLSM acts as non-contact surface profilometer, it is possible to do surface topography.

Confocal microscopy is shown to be a valuable tool for direct 3D visualization of particle dynamics in colloidal fluids and colloidal glasses. It provides information about particle motion and particle rearrangement that take place during the structural relaxation of liquids undergoing glass transition. CLSM investigations on hard-sphere suspensions undergoing glass transition have provided direct evidence for the existence of dynamical heterogeneities in the form of clusters of fast moving particles. No experiment has ever directly measured the size of crystal nuclei and its internal structure during crystallization. Using confocal microscopy, it is now possible to identify the size and internal structure of critical nuclei. The direct observation of the structure, dynamics and evolution of small crystallites using CLSM has allowed the characterization of the key process of nucleation and growth of colloidal crystals and to determine the important parameters that control this process.

Combination of static and dynamic light scattering techniques with CLSM is shown to characterize unambiguously the inhomogeneous nature of highly charged colloidal suspensions with particle sizes ranging over the visible range. CLSM could help us to unravel the nature of inhomogeneities (voids) in these suspensions and also in establishing the occurrence of gas-solid transition in these suspensions. Though the occurrence of gas-solid transition in bulk suspensions of highly charged colloids, provides evidence for existence of long-range attractive interaction in the interparticle interaction, the use of CLSM in imaging the particles in very dilute suspensions has helped in providing direct evidence for the existence of long-range attractive term in $U(r)$ of like-charged colloids. Colloidal crystals with lattice constants in the visible range serve as photonic crystals and are technologically important. Such applications require large single crystals with known orientation. Colloidal epitaxial process allows growing crystals with desired crystal orientation. Such ordered structures can be characterized by confocal microscopy.

The late stage of nucleation and growth process of a binary polymer mixture undergoing phase separation, where the minority phase droplets are quite polydisperse and have complicated morphologies, has been studied quantitatively using confocal fluorescence microscopy. Using this technique, it is easy to determine directly the domain size distribution and spatial correlations at various coarsening times. Further, the time evolution of a three dimensional spatially bicontinuous structure of a polymer

mixture undergoing the late stage of spinodal decomposition has been studied and the average local geometry of the interface is evaluated directly using CLSM. Such studies greatly enhance the understanding of phase separation phenomena not only in polymer mixtures but also in other macromolecular systems. From the results presented in this article it clearly emerges out that the laser light scattering and confocal laser scanning microscopy techniques are very useful investigative and characterizing tools to study a wide variety of phenomena in soft matter as well as in technologically important materials.

Acknowledgments

Authors wish to thank Dr. B Purniah for useful discussions. BVRT acknowledges Mr. P S Mohanty, Dr. J Yamanaka and Dr. T Sawada for very fruitful collaborative work.

References

[1] T Wilson *Confocal Microscopy* (ed) T Wilson (London : Academic) p1 (1990)

[2] C J R Sheppard and D M Shotton *Confocal Laser Scanning Microscopy* (Oxford, UK : BIOS Scientific) (1997)

[3] B V R Tata and Baldev Raj *Recent Advances in Materials Characterization* (eds) G Amarendra, Baldev Raj and M H Manghnani (Hyderabad : University Press) Ch. 5 (2006)

[4] B V R Tata and Baldev Raj *Bull. Mater. Sci.* **21** 263 (1998)

[5] P N Pusey and R J A Tough *Dynamic Light Scattering : Applications of Photon Correlation Spectroscopy* (ed) R Pecora (New York : Plenum) p85 (1985)

[6] B V R Tata *Proceeding of DAE-BRNS National Laser Symposium* (eds) A K Nath and K S Bartwal (New Delhi : Allied) p28 (2003)

[7] J K G Dhont, G Gompper and D Richter *Soft Matter : Complex Materials on Mesoscopic Scales* (eds) J K G Dhont, G Gompper and D Richter (Julich : Forschungszentrum) **Vol.10**, 11. 1 (2002)

[8] A K Arora and B V R Tata *Adv. Colloid Interface Sci.* **78** 49 (1998)

[9] B V R Tata *Curr. Sci.* **80** 948 (2001)

[10] P Steyger *Methods* **18** 435 (1999)

[11] G S Kino and G Q Xiao *Confocal Microscopy* (ed) T Wilson (London : Academic) p361 (1990)

[12] K Schatzel *J. Appl. Phys.* **B193** (1987); *ibid Proc. of the Int. Phys. Conf.* (ed) E Hilger **77** 175 (1985)

[13] D Magatti and F Ferri *Rev. Sci. Instrum.* **74** 1135 (2003)

[14] A P Y Wong and P Wiltzius *Rev. Sci. Instrum.* **64** 2547 (1993)

[15] B V R Tata, P S Mohanty, J Yamanaka and T Kawakami *Molecular Simulation* **34** 153 (2004)

[16] M Enmark, K Edsinger, G Lucas and G R Odette *J. Nucl. Mater.* **233** 347 (1996)

[17] J P H Sukamoto, W H Smyrl, N Casillas, M Al-Odan, P James, W Jin and L Douglas *Mater. Sci. Engg.* **A198** 177 (1995)

[18] T S Rao, A J Kora, B Anupkumar, S V Narasimhan and R Feser *Corrosion Sci.* **47** 1071 (2005)

[19] G R Odette, G E Lucas, E Donhue and J W Sheckherd *J. Nucl. Mater.* **233** 502 (1996)

[20] B V R Tata, P S Mohanty, M C Valsakumar and J Yamanaka *Phys. Rev. Lett.* (in press) (2004); B V R Tata *Phonons in Condensed Materials* (eds) S P Sanyal and R K Singh (New Delhi : Allied) p225 (2004)

[21] U Gasser, E Weeks, A Schofield, P N Pusey and D A Weitz *Science* **292** 258 (2001)

[22] W K Kegel and A Van Blaaderen *Science* **287** 290 (2000); *ibid* **287** 627 (2000)

[23] F H Stillnger *Science* **267** 1935 (1995); M D Ediger, C A Angell, and S R Nagel *J. Phys. Chem.* **100** 13200 (1996)

[24] W Kob, C Donati, S J Plimpton, P H Poole and S C Glotzer *Phys. Rev. Lett.* **79** 2827 (1997); C Donati *et al Phys. Rev.* **E60** 3107 (1999)

[25] M T Cicerone and M D Ediger *J. Chem. Phys.* **103** 5684 (1996)

[26] B V R Tata, P S Mohanty and M C Valsakumar *Phys. Rev. Lett.* **88** 018302 (2002)

[27] G Adam and J H Gibbs *J. Chem. Phys.* **43** 139 (1965)

[28] A J Hurd, N A Clark, R C Mockler and W J O'Sullivan *Phys. Rev.* **A26** 2869 (1982)

[29] J Derksen and W Van de Water *Phys. Rev.* **A45** 5660 (1992); M Hoppenbrouwers and W Van de Water *Phys. Rev. Lett.* **80** 3871 (1998)

[30] B V R Tata, E Yamahara, P V Rajamani and N Ise *Phys. Rev. Lett.* **78** 2660 (1997)

[31] J Yamanaka, H Yoshida, T Koga, N Ise and T Hashimoto *Phys. Rev. Lett.* **80** 5806 (1998)

[32] A Toyotama, T Sawada, J Yamanaka and K Kitamura *Langmuir* **19** 3236 (2003)

[33] P S Mohanty and B V R Tata *J. Colloid Interface Sci.* **264** 101 (2003)

[34] P S Mohanty, B V R Tata, A Toyotama and T Sawada *Langmuir* **21** 11678 (2005)

[35] B V R Tata, R Rajalakshmi and A K Arora *Phys. Rev. Lett.* **69** 3778 (1992); B V R Tata and A K Arora *Ordering and Phase Transitions in Charged Colloids* (eds) A K Arora and B V R Tata (New York : VCH) p140 (1996)

[36] R Van Roji, M Dijkstra and J P Hansen *Phys. Rev. E* **59** 2010 (1999); D Y C Chan, P Linse and S N Petris *Langmuir* **17** 4202 (2001)

[37] M N Tamashiro and H Schiessel *J. Chem. Phys.* **119** 1885 (2003); H N Von Grunberg, R Van Roji and G Klein *Europhys. Lett.* **55** 580 (2001)

[38] A E Larsen and D G Grier *Phys. Rev. Lett.* **76** 3862 (1996); *Nature* **385** 230 (1997)

[39] I Sogami and N Ise *J. Chem. Phys.* **81** 6320 (1984)

[40] J C Crocker and D G Grier *Phys. Rev. Lett.* **77** 1897 (1996)

[41] B V R Tata and N Ise *Phys. Rev.* **E61** 983 (2000)

[42] B V R Tata, P S Mohanty and J Yamanaka *STATPHYS22, 22nd International Conference on Statistical Physics (Banglaore, India)* Abstracts p89 (2004)

[43] A Van Blaaderen, R Ruel and P Wiltzius *Nature* **385** 321 (1997)

[44] A Van Blaaderen and P Wiltzius *Adv. Matter.* **9** 833 (1997)

[45] J P Hoogenboom, A Yethiraj, A K Van Langen-Suurling, J. Romijn and A Van Blaaderen *Phys. Rev. Lett.* **89** 256104 (2003)

[46] W R White and P Wiltzius *Phys. Rev. Lett.* **75** 3012 (1995)

[47] H Jinnai, T Koga, Y Nishikawa, T Hashimoto and S T Hyde *Phys. Rev. Lett.* **78** 2248 (1997)